International Journal of Engineering

J o u r n a l   H o m e p a g e :   w w w . i j e . i r

Numerical and Experimental Investigation of Motor Pressure Effect on Thermochemical Erosion of Graphite Nozzle in Solid Fuel Engines

E. Daneshfar[a], M. Aminy*[a], M. M. Doustdar[b], H. Fazeli[c]

[a] Material and Energy Research Center, Karaj, Iran
[b] Department of Mechanical & Aerospace Engineering, Imam Hussein University, Tehran, Iran
[c] Department of Mechanical Engineering, Malek Ashtar University of Technology, Tehran, Iran

P A P E R   I N F O

A B S T R A C T

Using heat shield, especially in throat area has a significant effect on combustion chamber pressure and thermal efficiency of solid fuel engines. Precise prediction of the regression of throat area for different pressures, will lead to optimal design of the motors, specifically for those of long burnout times. In this work, erosion of graphite nozzles employed in solid propellant motors with a specific composite propellant and variable pressures, is investigated. The numerical model utilized includes the Naiver-Stokes equations, chamber gas thermodynamic equations and thermochemical and heat conduction equations for the nozzle surface. In order to validate the numerical results, a cartridge type solid propellant motor with a graphite nozzle is experimentally tested. Using a 3D scanner in the experimental setup, the amount of inner surface regression for variable pressures (60, 90, 120 and 200 bars) is measured. Numerical and experimental results are in a proper conformity with each other. There is a direct relationship between convection heat transfer coefficient and the pressure. The overall erosion is the same for all four engine pressures. The erosion rate increases with increasing pressure. This rate for the fuel is about 0.21 mm/s for every 100 times the pressure up to 300 times. For a pressure higher than 300 times, a significant leakage occurs at the corrosion rate.

doi: *10.5829/ije.2019.32.11b.17*

NOMENCLATURE

H_{abl}	Ablative material enthalpy ($\frac{kJ}{kg}$)		K	Conduction Heat Transfer Coefficient ($\frac{W}{m.K}$)
$\dot{m}$	Ablative Material Mass Rate ($\frac{kg}{s}$)		V	Normal Velocity Component ($\frac{m}{s}$)
t	time (s)		h	Convection Heat Transfer Coefficient ($\frac{W}{m^2.K}$)
A	Conduction Heat Transfer Area (m^2)		L	Length (mm)
P	Pressure (Pa)		n	Burn Rate Pressure Exponent
r	radius (mm)		a	Burn Rate Coefficient ($\frac{m}{s}$)
R	Universal Gas Constant ($\frac{kJ}{kg.K}$)		r_d	diffusional reaction rate ($\frac{kg}{s}$)
T	Temperature (K)		r_k	kinetic reaction rate ($\frac{kg}{s}$)
D	Mass Diffusion Rate ($\frac{m^2}{s}$)		**Subscripts**	
$\dot{S}$	erosion Rate ($\frac{m}{s}$)		η	Coordinates perpendicular to the surface
s	erosion Amount (mm)		γ	Heat capacity ratio
y	Reactive Specie		$\dot{\omega}$	mass fraction of Species ($\frac{kg}{s}$)
U	Axial Velocity Component ($\frac{m}{s}$)		ρ	Density($\frac{kg}{m^3}$)
N_c	Species Count			

*Corresponding Author Email: mohammadaminy@merc.ac.ir (M. Aminy)

1. INTRODUCTION

Ablative shield materials play a pivotal role in high speed projectiles and specifically in solid propellant motors. Inner surfaces of these motors (specifically in the nozzle area) due to fuel combustion encounter severe condition of high temperatures applied in a short period of time. A high pressure and intensely turbulent flow is created as the temperature increases due to burning of propellant in the combustion chamber. The aforementioned flow can destroy strongest temperature resistant metals and alloys. Hence, it is important to protect the motor parts from severe conditions, in order to gain satisfactory performance. Due to these reasons many research works aim to design heat shield with high thermal efficiency to gain better thermal protection and projectile weight reduction. It is evident that shield materials during contact with high temperature and turbulent combustion gases, due to erosion phenomenon, will gradually disappear. The nozzle is the most vital part that encounters the high temperature gases.

Bianchi et al. [1-3] provided two different numerical methods in which they simulated and investigated erosion in nozzles with graphite shield material from different aspects. The first model was based on thermodynamic balance on the surface and the second one was based on the finite rate. They utilized diffusion functions for high temperature states and high aluminum powder percentage propellants and in converse condition with low temperature and low aluminum percentage propellants. Like other researcher, they declared three oxidants including of OH, H_2O and CO_2 as the most important factors of erosion of graphite shield materials in nozzles. These oxidants are the main products of the combustion that chemically react with graphite. There are other combustion products that due to their low mass percentages and having very minor effect on the erosion were not considered here.

Piyush and Vigor [4] studied the erosion in nozzles with metal throat area. They evaluated three metals having high melting temperatures including; Tungsten (W), Molybdenum (Mo) and Rhenium (Re). In order to avoid mechanical abrasion effect of Al₂O₃ on the total regression, an aluminum free hydroxyl-terminated poly butadiene (HTPB) propellant was utilized, so the erosion effect was pure thermochemical. They observed in all three cases that with rising the nozzle pressure from 70 to 450 bars, the regression rate notably increases [4].

One of the other methods of evaluating the regression in heat shields is the plasma arc method. The advantage of this method is namely the precisely adjustable system inlet temperature and having no time limit [5].

Currently, to design and build the nozzle throat area of solid propellant motors, graphite or carbon-carbon composites are mostly used. That was due to their mechanical properties such as; high strength in proportion to its weight, sublimation temperature and mechanical strength.

In recent years, many researches are devoted to investigating the effect of different parameters on the graphite erosion. In the research conducted by Ragini and Kenneth [6]; they have theoretically evaluated the effect of gas pressure on the graphite erosion using a computer code. In their work, they utilized two types of resin based composite HTPB propellants one of which had metal powders used as fuel components. They came to the conclusion that under the gas pressure of 140 bars, reactions are kinetically controlled and above that, reactions are controlled by diffusion.

Accomplished researches to date have mainly been using phenolic resin compounds as shield materials in regression phenomenon which is only applicable for low temperature cases or in less critical regions such as nozzle inlet and outlet but not for the throat area. Many resources [7-10] mainly due to instrumentals limitation and test condition have only carried out measurement of regression in the throat area but not on the whole nozzle length [11-14].

In this study to obtain comprehensive results, the effect of pressure on the erosion is investigated. For the experimental setup, the HTPB resin free propellant is used as motor fuel and the regression is precisely measured on the whole nozzle length. It should be noted that current research is planned to meet some demands of industry to the graphite heat shields.

2. MODELING AND GOVERNING EQUATIONS

Figure 1 shows the schematic of the flow field and the boundaries problem. The gas phase consists of a blend of various combustion gas components. Because of high heat transfer between the combustion gases and the nozzle surface in a short time, nozzle surface dramatically increases. Subsequently, chemical reactions occur between oxidizing components of combustion products and the nozzle surface (heat shield) which causes the regression of the surface. The amount of regression can be calculated by chemical reaction kinetic method.

2. 1. Governing Equations
For a variable coordinate system attached to the surface of the diminishing ablative material, temperature variations along the given points on the surface is attained from the following equation [9]:

$$\rho_s \frac{\partial h_s}{\partial t} = \frac{1}{A} \frac{\partial}{\partial r} \left(k_s A \frac{\partial T_s}{\partial r} \right) + \rho_s \dot{s} \frac{\partial h_s}{\partial r} \tag{1}$$

Assumptions considered for the physical model in Equation 1 are stated as follows:
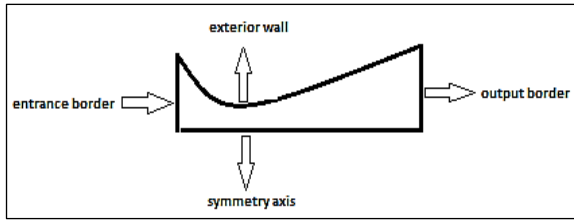
Figure 1. Schematic of the flow field and the boundaries

1. Thermodynamic properties are only a function of temperature.
2. The radiation heat transfer is negligible.
3. Graphite is considered as a homogenous material.
4. Conduction heat transfer in ablative material is one dimensional in the same direction with the nozzle radius vector.
5. The whole aluminum in the propellant is oxidized.
6. Carbon sublimation on the nozzle surface is negligible.

The terms provided in Equation (1) refer from left to right respectively to; stored sensible enthalpy, conduction heat transfer and energy flux due to moving coordinate. Because of the rapid heating of the surface, assuming the outer surface of the nozzle as adiabatic; therefore Equation (1) can be solved independent of the time. The aforementioned assumption is almost always valid in solid propellant motors.

2. 2. Gas to Solid Interface Boundary Layer   In order to accomplish the modeling of the erosion in gas to solid interface (combustion gases and graphite), mass and energy balance equations must be solved for every species. Equations (2) and (3) are the mass and energy balance equations, respectively.

$$\rho D_{im} \frac{\partial y_i}{\partial \eta}\Big|_w + \dot{\omega}_i = (\rho v)_w y_{iw} \qquad i = 1,...,N_c \tag{2}$$

$$k\frac{\partial T}{\partial \eta}\Big|_w + \sum_i^{N_c} h_{i_w}\rho D_{im}\frac{\partial h_i}{\partial \eta}\Big|_w + \dot{m}h_s =$$
$$(\rho v)_w h_w - k_s \frac{\partial T_s}{\partial r}\Big|_s \tag{3}$$

Basically, Equation (2) is conservation equation of mass on the ablative surface for the i specie. Terms on the left side of Equation (2) is the mass flux of the i specie into control surface attached to the ablative surface which is a result of diffusion and heterogeneous chemical reactions. The other term on the left ($\dot{\omega}_i$) is the production rate of species produced during the gas to solid interaction which takes positive sign for produced species and negative sign for consumed species.

Also, Equation (3) is, balance of energy on the surface. Left hand side terms of Equation (3), from left to right respectively, refer to energy flux into the control surface due to conduction of diffusive gases and ablative

surface movement. The terms on the right side of Equation (3), respectively from left to right, are the outlet heat flux from the control surface due to mass transfer and heat conduction into the ablative material [9,10].

Extending Equation (2) to all of the species and adding terms together results in Equation (4):

$$\sum_{i=1}^{N_c} \dot{\omega}_i = (\rho v)_w = \dot{m} = \rho_s \dot{s} \tag{4}$$

Substituting Equation (4) into Equation (3) yields the following equation:

$$k\frac{\partial T}{\partial \eta}\Big|_w - \dot{m}\Delta H_{abl} = -k_s\frac{\partial T_s}{\partial r}\Big|_s \tag{5}$$

where, ΔH_{abl} is the erosion enthalpy and its magnitude is gained by subtracting the total enthalpy of species in erosion process from the enthalpy of the solid graphite material at the ablative surface temperature.

The remaining boundary conditions are shown in Equation (6). The terms in Equation 6, from left to right respectively, refer to constant pressure on ablative surface, no slip condition and normal velocity which is equal to the regression rate.

$$\frac{\partial P}{\partial \eta}\Big|_\omega = 0 \quad , u = 0 \quad , v = \dot{m}/\rho \tag{6}$$

2. 3. Chemical Reactions   Graphite or carbon-carbon composite used as heat shield in the throat area of solid propellant motor nozzle encounters chemical reaction and gradually consumed. Products of combustion of the solid propellant consist of $AlCl$, $AlCl_2$, H_2O, OH, CO_2 , Fl_2O and N_2OH. Among the mentioned species, according to various resources in the literature, OH , H_2O and CO_2 are the main species that react with carbon. The reaction formulas are as follows:

$$C_s + H_2O \rightarrow CO + H_2$$
$$C_s + CO_2 \rightarrow 2CO \tag{7}$$
$$C_s + OH \rightarrow CO + H$$
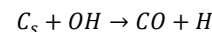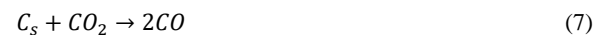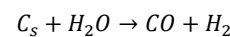
It's worth mentioning that these reactions are mainly of kinetic type but not diffusional [9,10].

In general, rate of a reaction is defined by the following equation [3]:

$$1/r = 1/r_d + 1/r_k \tag{8}$$

In which r_d and r_k are diffusional and kinetic reaction rates, respectively. If the kinetic reaction rate be much greater than the diffusional reaction rate, then the reaction is essentially controlled by the diffusion and vice versa.

According to some references in the literature in the field of erosion of graphite [3, 5, 6], when the combustion gas temperature is less than 2800 °C, the reaction is kinetic and when above that, the diffusion is the dominant effect. It is worth mentioning the experimental data approve this fact.

Owing to the fact that in our problem the combustion gas temperature in the throat area is less than the mentioned limit (i.e. 2800 ℃), hence the reaction can be considered kinetic. So the mass loss rate is defined by the following equation [1, 4]:

$$\dot{m}_i = p_i^n . A_i . T_w^b . \exp\left(-\frac{E_i}{RT_w}\right) \tag{9}$$

where, $\dot{m}_i$: Carbon surface mass loss rat
p_i: Partial pressure of species
E_i: Activation energy of heterogeneous reaction
A_i, b, n: Non dimensional constants (available in the literature)
T_w: Carbon surface temperature in Kelvin
R: Universal gas Constant
All of the kinetic parameters of Equation (9) are available in Table 1.
Total erosion of graphite in accordance with the exhaust gases is calculated by Equation (10).

$$\dot{m}_i = \dot{m}_{H_2O} + \dot{m}_{CO_2} + \dot{m}_{OH} = \rho_s . \dot{s} \tag{10}$$

where ρ_s is the graphite density and $\dot{s}$ is the erosion rate in m/s.

TABLE 1. Kinetic data of the surface reaction

	n	b	$E_i, Kcal/mole$	A_i
CO_2	0.5	0	68.8	480000
H_2O	0.5	0	68.1	9000
OH	1	-0.5	0	361

3. NUMERICAL SOLUTION

Mass production rate terms $\dot{\omega}$ for the species produced during erosion of heat shield are provided in Equations (11) to (17).

$$\dot{\omega}_{co} = \dot{m}_{H_2O}\left(\frac{w_{co}}{w_c}\right) + \dot{m}_{CO_2}\left(\frac{2w_{co}}{w_c}\right) + \dot{m}_{OH}\left(\frac{w_{co}}{w_c}\right) \tag{11}$$

$$\dot{\omega}_{co_2} = -\dot{m}_{CO_2}\left(\frac{w_{CO_2}}{w_c}\right) \tag{12}$$

$$\dot{\omega}_{H_2O} = -\dot{m}_{H_2O}\left(\frac{w_{H_2O}}{w_c}\right) \tag{13}$$

$$\dot{\omega}_{OH} = -\dot{m}_{OH}\left(\frac{w_{OH}}{w_c}\right) \tag{14}$$

$$\dot{\omega}_{H} = \dot{m}_{OH}\left(\frac{w_H}{w_c}\right) \tag{15}$$

$$\sum \dot{\omega}_i = \dot{m} = \rho.\dot{s} \tag{16}$$

$$p_i = y_i.p.\left(\frac{w}{w_i}\right) \tag{17}$$

Figure 2 schematically shows steps toward solving the problem. The steps include motor design, input parameters specification, running numerical codes, calculating demanded parameters for evaluating the amount of ablative material etc. This flowchart is comprised of four main parts including motor analysis, viscous nozzle flow solution, determination of chemical reactions influencing the erosion and numerical codes.
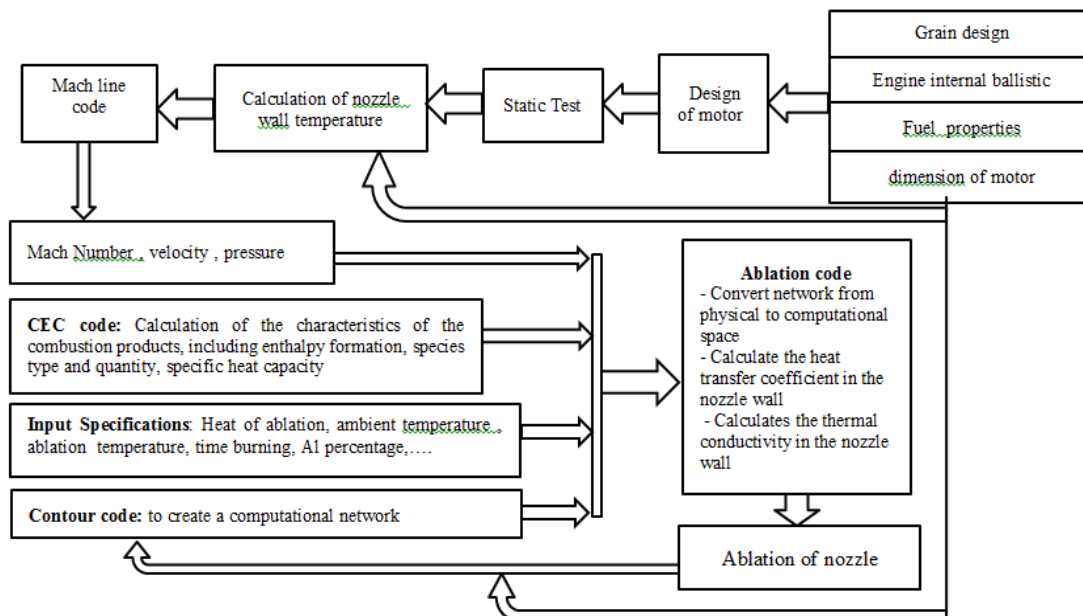
Figure 2. Main flowchart of solving the problem

4. STANDARD MOTOR CHARACTERISTICS

Due to high price and safety problems of complete solid propellant motors, tests on solid propellant properties, normally a standard motor is used to investigate heat shields and insulators characteristics and motor analysis. Bodies of standard motors are made of steel material and mechanically designed so that all parts can endure very high pressures. Effortlessly being capable of disassembling and reassembling motor parts and cleaning them is another advantage of employing standard motors. In order to measure different parameters, a number of holes are considered on its body. Moreover, in standard setups usually nozzle convergence and divergence angles are 45 and 15, respectively. Standard motor characteristics in current work are available in Table 2 [15, 16].

To study the effect of motor pressure on the erosion of graphite nozzles, four different standard motors of different pressures and the same solid propellant type (A15) are employed. Solid propellant characteristics utilized in these motors are indicated in Table 3.

TABLE 2. Propellant Characteristics

Propellant Characteristics	A15
Resin percentage	19
Ammonium perchlorate percentage	65.5
Aluminum percentage	15
Other component percentage	0.5
γ	1.2025
ρ	$1770(^{kg}/_{m^3})$
R	$299.7(^{kJ}/_{kg.K})$
T	$3300(^{\circ}C)$
(burning rate pressure exponent) n	0.182
(coefficient of pressure) a	0.00423

**TABLE 3.** Geometrical and thermodynamic parameters of the four standard motors

Motor Pressure [bar]	60	90	120	200
Propellant type	A15	A15	A15	A15
Nozzle Throat Diameter [mm]	33.9	28	25.7	22
Nozzle Inlet Diameter [mm]	135	135	135	135
Nozzle Outlet Diameter [mm]	47.16	47	46.7	40
Propellant Mass [kg]	6	6	6	6
Initial Propellant Temperature (°C)	31.5	32	32	32.5

5. NUMERICAL RESULTS

Figure 3 shows the nozzle wall temperature along the flow direction for four different pressures (60, 90, 120 and 200 bars). For the all pressures ranges and within the converging area of nozzle, the temperature is remained constant. Along the throat and diverging zone, however, the temperature gradually decreases. Basically, at the inlet, the nozzle wall temperature is the adiabatic flame temperature (2950 K) although at the outlet it takes lower values of about 2750 K. Moreover, maximum temperature reduction corresponds to pressure at 200 bars and minimum temperature reduction corresponds to pressure 60 bars. The interpretation of the behavior of the nozzle wall temperature is such that at the entrance, because of the change pressure to velocity, the temperature of the wall is almost constant, and at the divergent area due to the change of the flow regime from subsonic to ultrasonic and increasing in the cross-section of the nozzle, the energy of the fluid convert to momentum, so the bulk temperature of fluid decreases and also wall temperature also decreases.

Figure 4 shows heat transfer coefficient distributions for various pressures along the length of the nozzle. As it can be seen from the diagram, within the convergent area the convective coefficient has increasing trend, at the divergent area reducing trend and the inlet of the throat is maximum. In general, all along the nozzle area the rate of convective coefficient at 200 bars pressure has highest value and at 60 bars it has the least value. It should be noted that changing the coefficient of convection along the nozzle is directly related to the intensity of fluid flow. Because the flow rate is a function of the cross-sectional area of the fluid, it increases from the entrance to the throttling and decreases from the throttling to the next.

Figures 5 and 6 show the mass fractions of CO_2 and H_2O with respect to pressure. As it was explained earlier, OH, H_2O and CO_2 are the combustion products which contribute to the erosion of graphite. But the OH amount in intended propellant is very small and negligible.
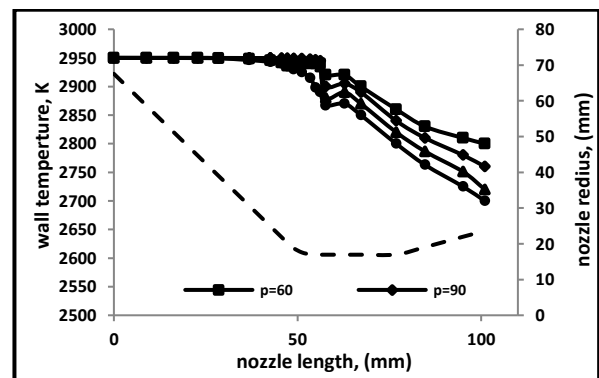
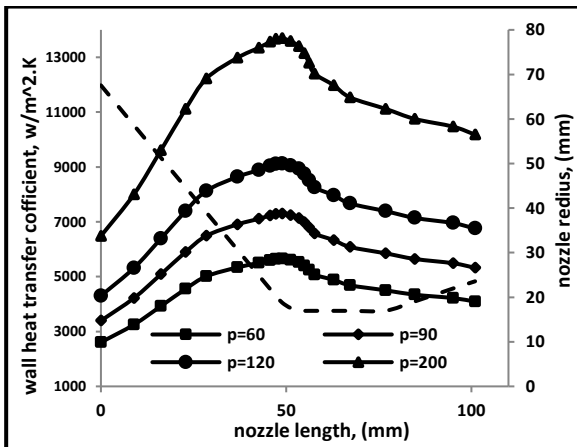**Figure 3.** Nozzle wall temperature distributions

Figure 4. convection heat transfer coefficient distributions along the nozzle
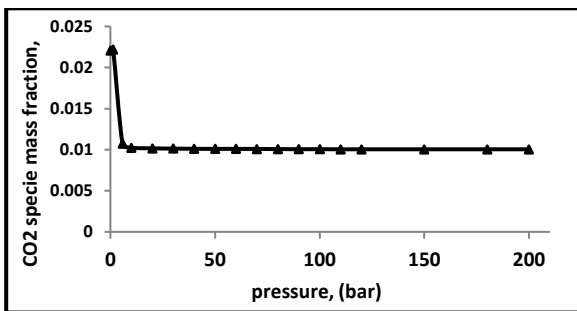

Figure 5. CO_2 percentage distribution in accordance with pressure
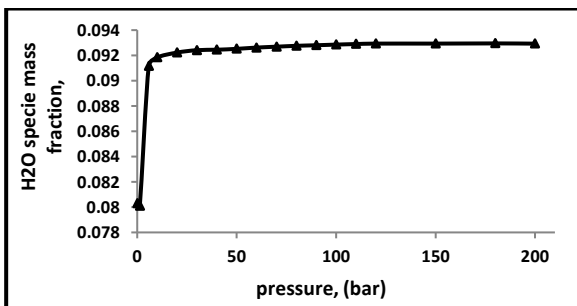

Figure 6. H_2O percentage distribution in accordance with pressure

According to Figure 5, for pressures lower than about 10 bars the diagram has a negative slope and for higher pressure ranges, CO_2 percentage maintains a constant value. For H_2O percentage (Figure 6), contrariwise, for under 10 bars range, the diagram has a positive slope and then suddenly converges to a rather constant value.

The concentration of H_2O and CO_2 in the combustion chamber is roughly independent of pressure and temperature. But it changes in length of nozzle due to changes in temperature and pressure, especially divergence zone. Because the possibility of changing

species to each other in the event of temperature and pressure changes.

Figure 7 shows the numerical graphite surface erosion variation along nozzle for different pressures. The diagram reveals that the erosion amounts are almost the same for all pressure ranges. Although a slight and not noticeable difference is seen in the diverging zone. The amount erosion at the entrance of the nozzle throat is at its highest of 0.77 for all motors.

The most important result obtained from previous diagrams is that despite large differences in convective heat transfer coefficients for all pressure ranges, the erosion amount was almost the same. It is important to notice that the curves in Figure 7 are total erosion after the propellant complete burned and propellant masses of all motors are the same. For instance in a propellant case of high pressure, the burn time reduced. Since the propellant mass for all the motors are the same. Hence, the final erosion for the motors are near to each other.

The erosion rate distribution along the nozzle for different pressures is shown in Figure 8. The burn time is ½ s for all of the pressure ranges. It is obvious that the propellant mass and outlet flow rates are different for variable pressures; the higher the pressures the higher the outlet flow rate and vice versa. As it is seen from the diagram, higher erosion rates are gained for higher pressures and the curves reach their maximum in the throat area. It should also be noted that under the pressure of 300 bars, there is a slight increment between the curves although above that pressure a sudden jump is seen. For instance by comparison the erosion rate all the nozzle throat for 300 and 500 bars pressure, it can be seen that the pressure increases by 66 percent, where as erosion rate can vary by 100 percent.

6. EXPERIMENTAL RESULTS

In order to carry out the experimental tests, a special static test bed for solid fuel, consisting of pressure and trust gages was used. The measurement accuracies are
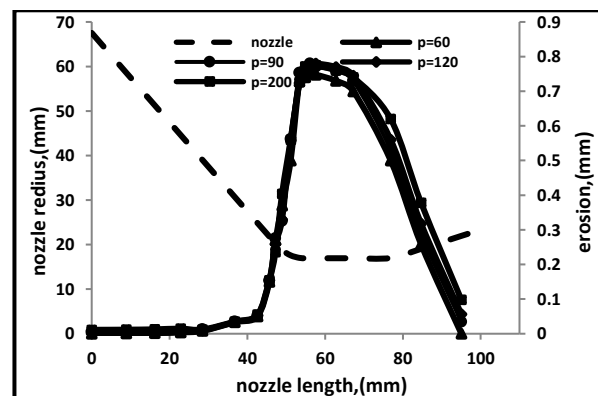

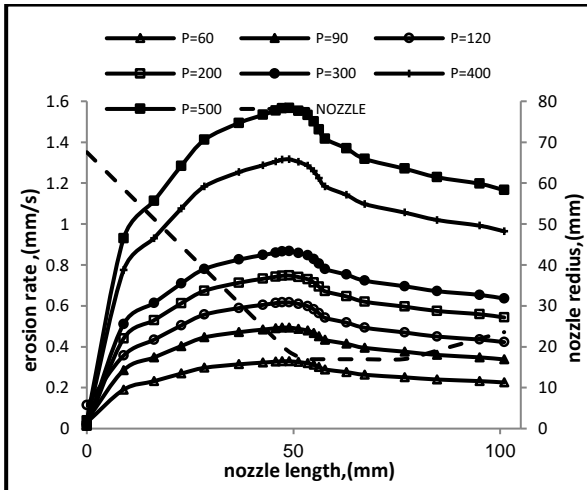**Figure 7.** Numerical graphite surface erosion amount along the nozzle

Figure 8. Numerical erosion rate distributions for different pressures

0.001 bar for pressure, 1N for thrust and 0.1K for temperature. Also data reading frequency was 1000 Hz. Moreover, to confirm the output data with confidence, tests were repeated several times.

The graphite shell utilized as heat shield in the tests is shown in Figure 9. In order to measure the amount of erosion, a 3D scanner with an accuracy of 0.01mm is employed. The scanner measured the graphite part dimensions before and after the erosion so as to calculate the total erosion amount.

Figures 10 to 13 show the thrust and the pressure change with respect to time for each of the four motors. Units for thrust, pressure and time are kg_f, bar and mms, respectively. The motors characteristics are available in Table 3. It should be noted that output pressure naming the diagrams is the average neutral pressure of the motor chamber. Having equal amount of propellant mass in all of the motors, the sweeping area under the curves are rather the same, hence as previously mentioned, higher pressures lead to lower burnout times.

The experimental total erosion of the nozzles surface along the nozzles length for the four motors is depicted in Figure 14. It can be seen that after turning of the motor, the erosion amount for each case is almost the same only at entrance and exit small difference are observed.
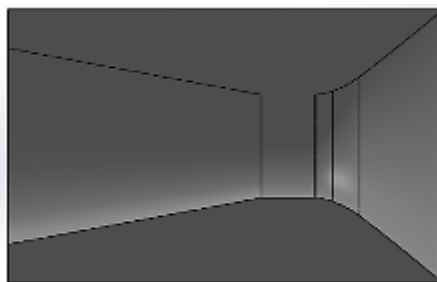

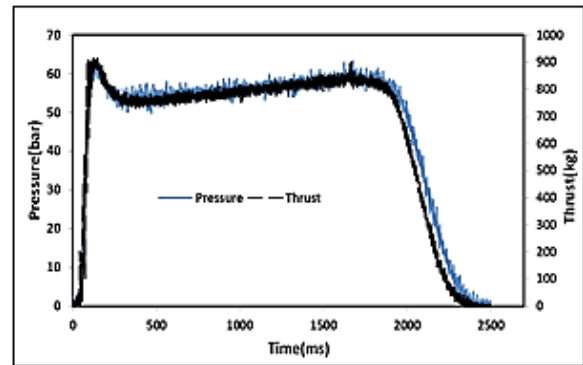**Figure 9.** The graphite employed in the tests

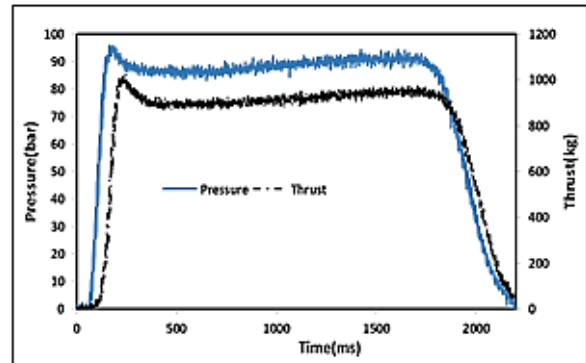**Figure 10.** Chamber pressure with time for 60bar

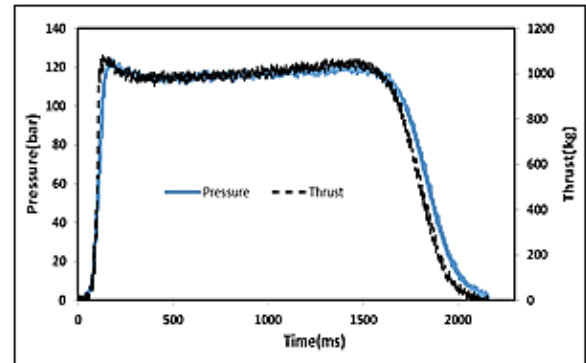**Figure 11.** Chamber pressure with time for 90bar

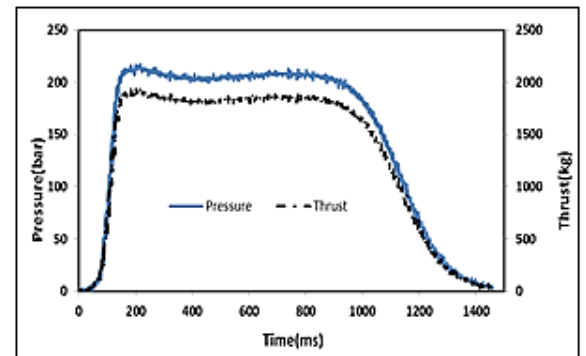**Figure 12.** Chamber pressures with time for 120bar

Figure 13. Chamber pressure with time for 200bar

The important thing to be referred to in this diagram, is that around the throat area, the slopes of the curves are very high but those in other zones are much lower. Comparing the numerical and experimental results diagrams (Figures 7 and 14), it is evident that in the diverging zone of the nozzle or after the peak of the curves, they do correspond with each other. Indeed the experimental results show significantly higher slopes at the throat outlet compared with numerical data. This controversy can be referred to the effect of inertial forces that cause the flow separation. Actually, the flow separation is not tracked in the numerical modeling of the problem.

Maximum experimental erosion amount and heat transfer coefficient in entrance of nozzle for the four pressure ranges is indicated in Figure 15. It's evident that the erosion does not noticeably changed with pressure and is around 0.74 on the entire range. But the relation of heat transfer coefficient and pressure is linear and it increase by increasing the pressure.

Figure 16 compares the experimental and numerical results for the maximum erosion rates in the throat area. Maximum deviation in the results is about 0.03 mm/s which correspond to around 4 percent of the total erosion of the graphite heat shield. The diagram indicates a linear relation between erosion rate and it is true for experimental and numerical results.
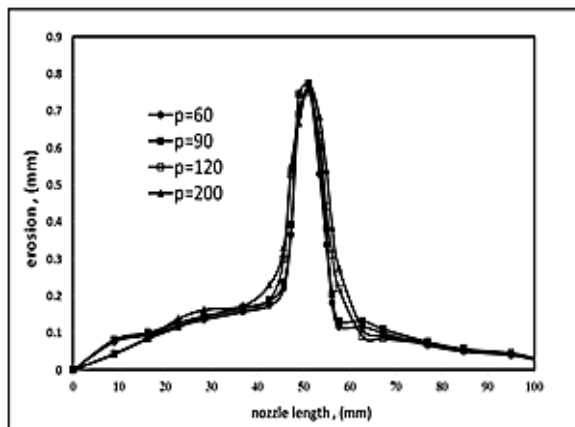

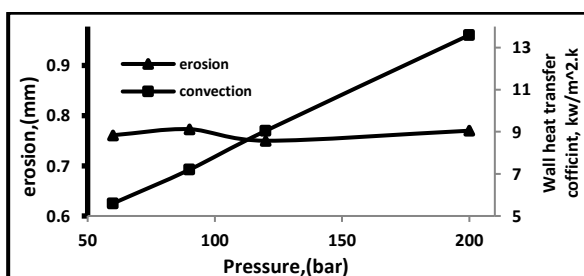**Figure 14.** Experimental graphite surface erosion amount along the nozzle

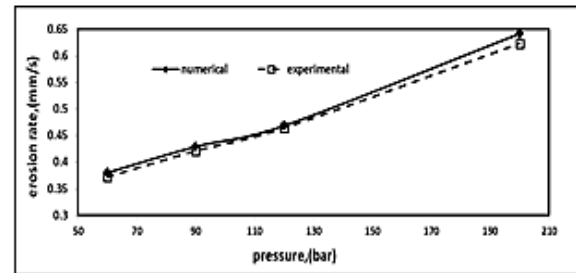**Figure 15.** Experimental maximum erosion amount of the nozzle surface

Figure 16. Comparisons between numerical and experimental results for the maximum erosion rates

7. CONCLUSION

To sum up, considering all of the above-mentioned observations and the comparison made between numerical and empirical results, the results can be summarized as follows:

1. The nozzle surface temperature is almost constant in the converging zone. It decreases with a rather high slope in the throat area and keeps decreasing trend in the divergence zone.
2. The nozzle surface temperature does not significantly change with pressure.
3. There is a direct relationship between convection heat transfer coefficient and the pressure.
4. The total erosion amount of propellant mass the total erosion amount along the nozzle is almost constant for different pressures ranges, although in the divergence zone a slight difference is observed.
5. The increment of pressure causes the increment of the erosion rate. For A15 propellant this rate increases by 0.21mm/s for each 100 bars increment of pressure for pressures lower than 300 bars. Above 300 bars a sudden increment is seen in the erosion rate.

8. ACKNOWLEDGEMENT

9. REFERENCES

1. Bianchi, D. and Neri, A., "Numerical simulation of chemical erosion in vega launcher solid-propellant rocket motor nozzles", in 51st AIAA/SAE/ASEE Joint Propulsion Conference., (2015), 4175.

2. Bianchi, D., Nasuti, F., Onofri, M. and Martelli, E., "Thermochemical erosion analysis for carbon-carbon rocket nozzles", in 45th AIAA/ASME/SAE/ASEE Joint Propulsion Conference & Exhibit., (2009), 4977.

3. Bianchi, D. and Nasuti, F., "Thermochemical erosion analysis of carbon-carbon nozzles in solid-propellant rocket motors", in 46th

AIAA/ASME/SAE/ASEE Joint Propulsion Conference & Exhibit., (2010), 7075.

4. Thakre, P. and Yang, V., "Chemical erosion of refractory-metal nozzle inserts in solid-propellant rocket motors", *Journal of Propulsion and Power*, Vol. 25, No. 1, (2009), 40-50.

5. Kumar, S., Kushwaha, J., Mondal, S., Kumar, A., Jain, R. and Devi, G.R., "Fabrication and ablation testing of 4d c/c composite at 10 mw/m2 heat flux under a plasma arc heater", *Materials Science and Engineering: A*, Vol. 566, (2013), 102-111.

6. Acharya, R. and Kuo, K.K., "Effect of pressure and propellant composition on graphite rocket nozzle erosion rate", *Journal of Propulsion and Power*, Vol. 23, No. 6, (2007), 1242-1254.

7. Turchi, A., Bianchi, D., Nasuti, F. and Onofri, M., "A numerical approach for the study of the gas–surface interaction in carbon–phenolic solid rocket nozzles", *Aerospace Science and Technology*, Vol. 27, No. 1, (2013), 25-31.

8. Turchi, A., Bianchi, D., Thakre, P., Nasuti, F. and Yang, V., "Radiation and roughness effects on nozzle thermochemical erosion in solid rocket motors", *Journal of Propulsion and Power*, Vol. 30, No. 2, (2014), 314-324.

9. Kianifar, A. and Mohammadiun, H., "Numerical analysis of thermal conductivity of non-charring material ablation carbon-carbon and graphite with considering chemical reaction effects, mass transfer and surface heat transfer", in ASME 2010 3rd Joint US-European Fluids Engineering Summer Meeting collocated with 8th International Conference on Nanochannels, Microchannels, and Minichannels, American Society of Mechanical Engineers., (2010), 335-340.

10. Lyon, R.E., "Pyrolysis kinetics of char forming polymers", *Polymer Degradation and Stability*, Vol. 61, No. 2, (1998), 201-210.

11. Dimitrienko, Y.I. and Dimitrienko, I., "Effect of thermomechanical erosion on heterogeneous combustion of composite materials in high-speed flows", *Combustion and Flame*, Vol. 122, No. 3, (2000), 211-226.

12. Peng, L.-n., He, G.-q., Li, J., Wang, L. and Qin, F., "Effect of combustion gas mass flow rate on carbon/carbon composite nozzle ablation in a solid rocket motor", *Carbon*, Vol. 50, No. 4, (2012), 1554-1562.

13. Shen, X.-T., Liu, L., Li, W. and Li, K.-Z., "Ablation behaviour of c/c–zrc composites in a solid rocket motor environment", *Ceramics International*, Vol. 41, No. 9, (2015), 11793-11803.

14. Hui, W.-H., Bao, F.-T., Wei, X.-G. and Liu, Y., "Analysis of ablative performance of c/c composite throat containing defects based on x-ray 3d reconstruction in a solid rocket motor", *International Journal of Turbo & Jet-Engines*, Vol. 32, No. 4, (2015), 351-359.

15. Sutton, G.P. and Biblarz, O., "Rocket propulsion elements, John Wiley & Sons, (2016).

16. Davenas, A., "Solid rocket propulsion technology, Newnes, (2012).

Numerical and Experimental Investigation of Motor Pressure Effect on Thermochemical Erosion of Graphite Nozzle in Solid Fuel Engines

E. Daneshfar[a], M. Aminy[a], M. M. Doustdar[b], H. Fazeli[c]

a Material and Energy Research Center, Karaj, Iran
b Department of Mechanical & Aerospace Engineering, Imam Hussein University, Tehran, Iran
c Department of Mechanical Engineering, Malek Ashtar University of Technology, Tehran, Iran

چکیده

کاربرد سپرهای حرارتی در گلوگاه موتورهای سوخت جامد، به دلیل تاثیر خوردگی این ناحیه بر فشار محفظه احتراق و نهایتا بازده حرارتی موتور، موجب مطالعه زیادی در این حوزه گردیده است. پیش بینی صحیح مقدار پسروی سطح گلوگاه در فشارهای مختلف، منجر به طراحی بهینه موتور، بویژه در موتورهایی با زمان سوزش بالا می‌گردد. در این تحقیق، خوردگی نازل گرافیتی در موتورهای سوخت جامد برای یک سوخت مرکب با ترکیب خاص، در فشارهای مختلف مورد بررسی قرار گرفته است. مدل عددی استفاده شده، شامل حل معادلات ناویر استوکس جریان سیال، معادلات ترمودینامیکی داخل موتور، معادلات ترموشیمی و هدایت حرارتی سطح نازل می‌باشد. جهت اعتبارسنجی نتایج مدل عددی، یک موتور سوخت جامد کامل از نوع کارتریجی با نازل گرافیتی مورد آزمایش قرار گرفته است. همچنین توسط دستگاه اسکنر سه بعدی مقدار خوردگی سطح داخلی نازل برای فشار کارکرد ۶۰ ، ۹۰، ۱۲۰ و۲۰۰ بار ندازه‌گیری شده است. مقایسه نتایج حاصله بیانگر مطابقت خوب خروجی مدل عددی با داده های تجربی در گلوگاه و حوالی آن می باشد. ما بین ضریب انتقال حرارت و فشار رابطه مستقیم دارد. خوردگی کلی برای هر چهار موتور یکسان است. نرخ خوردگی با افزایش فشار، افزایش پیدا می کند. این نرخ برای سوخت در حدود ۰/۲۱ میلی متر بر ثانیه به ازا هر ۱۰۰ بار افزایش فشار تا محدوده ۳۰۰ بار می باشد. برای فشار بالاتر از ۳۰۰ بار یک جهش قابل توجه در نرخ خوردگی ایجاد می گردد.

doi: 10.5829/ije.2019.32.11b.17